Structural Preferences, Argon Nanocoating, and Dimerization of *n*-Alkanols As Revealed by OH Stretching Spectroscopy in Supersonic Jets[†]

Tobias N. Wassermann, Philipp Zielke, Juhyon J. Lee, Christine Cézard, and Martin A. Suhm*

Institut für Physikalische Chemie, Universität Göttingen, Tammannstrasse 6, 37077 Göttingen, Germany

Received: February 5, 2007; In Final Form: March 27, 2007

n-Alkanols can occur in a multitude of energetically competitive conformational states. Using the OH stretching vibration as an infrared and Raman spectroscopic sensor in supersonic jet expansions, the torsional preferences around the C_α–O and C_β–C_α bonds are probed for *n*-propanol through *n*-hexanol. Raman detection is more powerful for isolated monomers, whereas IR spectroscopy is more sensitive for molecular complexes. The subtle IR vibrational shift induced by the nanocoating of *n*-alcohols with Ar atoms is shown to alternate with chain length. A large number of alcohol dimer absorptions is observed and subjected to collisional relaxation and nanocoating conditions. Essential features of the dimer spectra are modeled successfully by a simple force field approach. Exploratory quantum chemical calculations up to the MP2/aug-cc-pvqz level encourage a rigorous theoretical study of the subtle conformational aspects in monomers and possibly also in dimers of linear alcohols.

1. Introduction

Extended alkyl chains show a rich torsional isomerism around the non-terminal C–C bonds, which grows exponentially with chain length. Subtle conformational equilibria among the rotamers[1] shape the properties of membranes[2] and surfaces,[3] and it is desirable to characterize them in detail, in particular for alkyl chains which are terminated by a functional group. A simple and important example for end-derivatized and thus amphiphilic alkanes are *n*-alkanols.[4] Their anesthetic power and membrane interactions are of much interest.[5,6] *n*-Octanol is the reference compound for the partition of anesthetic and other compounds between aqueous and organic media.[7] The sensorial potential of the OH group for molecular conformations is well-established,[8] even at room temperature. It becomes progressively powerful if thermal effects are reduced by cooling the molecules in supersonic expansions.

Supersonic jet expansion is also the method of choice for the generation and study of isolated dimers.[9–12] Dimers represent the primary and thus crucial step for the aggregation of chain molecules into mesoscopic membranes,[2] surfaces,[3] and also crystals.[13] The aggregation effects on the hydrogen-bonded OH stretching vibration are substantial[9] and invite a range of modeling approaches.[14] A more subtle effect is caused by the aggregation of Ar atoms around the alcohol molecules,[15] which can mimic the perturbation of a bulk Ar matrix isolation environment.[16,17] This nanocoating process can be probed in a supersonic expansion by addition of varying amounts of Ar to the He carrier gas.[15] The resulting Ar nanomatrix is certainly less exotic and exciting than a superfluid He nanodroplet environment,[18] but it provides interesting connections between spectra in the gas phase and in bulk matrix isolation.

Besides condensation on the polarizable alcohol molecules, Ar can assist the structural relaxation[19] of metastable chain conformations into more stable local minima and into the global minimum over not too high barriers.[15] This is due to the larger mass and volume of Ar as compared to He, which enhances inelastic collision events.

Supersonic jet studies of linear alcohols beyond ethanol are rare.[9,10,14] Studies in a variety of condensed phases are more abundant,[5,20–25] but they do not allow for a clear-cut separation of intramolecular and intermolecular effects on the conformation. Even in condensed phases, there have been some indications that the fully stretched all-trans conformation of *n*-alkanols[25] is challenged by conformations involving a gauche conformation along the C_α–C_β bond. Van der Waals interactions of the oxygen atom with C_γH have been postulated as a reason.[21] However, it was shown that even a mild perturbation such as matrix embedding can change conformational preferences in alcohols in a dramatic way.[15,17] Furthermore, the related alkyl chlorides with a similar van der Waals interaction possibility show a trans preference for the C_α–C_β bond, except for the hexyl chloride under special conditions.[26] In room temperature solution phases, most of the chain length effects on the alcohol conformation and aggregation are washed out in the infrared spectrum,[5] at least in the OH stretching range.

In the crystalline solid state, periodicity requirements reduce the torsional diversity of *n*-alkanols to one or two out of the many possible conformations.[15,21,22,25] However, these conformations are dictated more by intermolecular and packing effects than by the intrinsic stability of the monomer structure. Therefore, the conformation often changes between different polymorphic forms.[4] This can lead to chain length alternations in melting points[27] and other phase transitions.[4]

Microwave (MW) spectroscopy is probably the method of choice for the detailed characterization of isolated alcohol monomer conformations,[28] also for astrochemical use.[29] However, the associated assignment effort does not scale favorably with system size. For *n*-propanol, there is a significant amount of MW work available (see refs 29 and 30 and references cited therein). Unless specific resonances between states centered on different conformations provide very accurate energy differences

---

between the conformations,[29,31,32] information on conformational energy differences is usually extracted from spectral intensities. This is more difficult in the high-resolution MW approach than for a more coarse-grained, vibrationally resolved technique. Therefore, the vibrational characterization of conformational preferences in alcohols can assist further MW studies, by identifying robust chain length trends.

Some quantum chemical studies of the shorter *n*-alkanols and their clusters are available. For *n*-propanol monomers, they approach spectroscopic accuracy,[33] whereas for *n*-butanol[21,24] and in particular for its clusters,[24] they are very exploratory in character. A major purpose of the present work is to encourage highly accurate quantum chemical studies of the conformational landscape of *n*-alcohols, by providing experimental constraints and evidence for interesting chain length trends for some of these elementary conformational issues in organic chemistry.

For this purpose, our first experimental results on subtle influences of Ar relaxation, Ar nanocoating, and self-dimerization on conformational aspects of *n*-alkanol molecules will be outlined. The first Raman jet spectra of these systems are presented. Molecular modeling and quantum chemical calculations are explored to provide some initial feedback for the interpretation of the spectra. As we will show, there is room for improvement in capturing some subtle yet essential aspects of the energetics and spectroscopy of linear alcohols.

After a brief summary of the experimental and computational techniques in section 2, section 3 presents and discusses the results for alcohol monomers. Section 4 deals with the dimer spectra. A summary and outlook is given in section 5.

2. Methods

The measurement of *n*-alkanol (ROH) monomer and dimer OH stretching IR spectra in supersonic jet expansions closely follows the procedure described in ref 15 for ethanol but uses the more sensitive filet-jet setup throughout.[11,12] He/Ar/ROH gas mixtures are prepared by bubbling a rare gas or rare gas mixture through a thermostatted saturator containing the liquid ROH. Variation of the Ar content affects the extent of conformational relaxation and coating of the monomers and clusters. The higher price of the more polarizable gases Kr and Xe currently prevents their use in related experiments. The gas mixture is collected in a 67 L reservoir, from which it is admitted through six high-throughput pulsed magnetic valves into a pre-expansion chamber. The pre-expansion chamber is separated from the main 23 m^3 vacuum chamber by a 600 mm $\times$ 0.2 mm slit. The flow through this extended slit becomes supersonic and adiabatically cools the gas mixture. Typical translational/rotational temperatures are below 20 K. Vibrational and conformational temperatures can be much higher and nonuniform as a result of less efficient collisions and sizable isomerization barriers. The mildly focused, modulated beam from a purged Bruker Equinox 55 Fourier transform infrared (FTIR) spectrometer traverses the extended zone of silence of the supersonic expansion in a distance of 10 mm from the nozzle exit, where the influence from the background gas is minimized. The IR beam attenuation is probed by a large area InSb detector.[12] The pulsed expansion is synchronized to the 2 cm^{-1} 100 ms FTIR scan, thus providing an entire IR spectrum in a single pulse. A higher spectral resolution[34] can be achieved[35] but is of little use in the present application. It would decrease the S/N ratio without benefit for the band profiles, which arise from residual rotational structure and IVR processes. To optimize the S/N ratio, an optical filter (2860−4000 cm^{-1}) is used. In the monomer region, the baseline quality is often limited

by imperfect compensation of atmospheric water traces. We note that the samples themselves do not contain significant amounts of water, such that mixed complex formation is suppressed to a large extent. For propanol, weak absorptions due to mixed complexes with water have been identified in water-rich expansions near 3670 and 3546 cm^{-1}, close to but not identical with propanol monomer and dimer absorptions. We can safely exclude that any of the reported cluster absorptions in this contribution involve water. The large vacuum chamber ensures that despite a gas flow of up to 1 mol per pulse, the background pressure does not interfere with the expansion zone of silence. After (and during) the pulse, the background gas is pumped away by a series of mechanical pumps (2500 m^3/h). After typically 20 s, the pulse/recovery cycle is repeated. In some experiments, the vacuum chamber was reduced to 8 m^3 and the pumping speed was only 500 m^3/h to share resources with another jet experiment. This enforces longer waiting times between pulses up to 80 s but leads to otherwise equivalent spectra. An inherent drawback of the non-evacuated FTIR spectrometer is the presence of imperfectly compensated atmospheric water lines in the alcohol monomer region. A technique which only samples the jet region such as Raman scattering does not suffer from this limitation.

Spontaneous Raman scattering spectra were recorded with a recently developed supersonic jet setup.[36] The gas mixtures are prepared in the same way as for the FTIR measurements and are collected in a 67 L reservoir. The gaseous samples are expanded through a 4.0×0.1 mm^2 slit nozzle into the expansion chamber. The expansion is controlled by a high-throughput pulsed magnetic valve. The expansion chamber is evacuated by a Roots pump (250 m^3/h) which is backed up by a rotary vane pump. The beam of an 18 W Coherent Verdi V18 laser (in some cases a 5 W Verdi or a 10 W Spectra Physics laser) is focused on the center of the expansion along the slit. The theoretical beam waist approaches 80 μm. The scattered light is collected by an achromatic planoconvex lens (Ø = 50 mm, f = 150 mm) using a 90° geometry. To enhance the signal the light scattered in a 270° angle is reflected by a spherical mirror through the scattering center onto the collecting lens. The collecting lens forms a collimated beam of light which is sent through a holographic notch filter (Kaiser Optical Systems, Inc., Ø = 55 mm) to remove elastically scattered 532 nm photons. The inelastically scattered photons are focused on the entrance slit of a McPherson model 2051 monochromator (f = 1000 mm, f/8.7, 1200 gr/mm grating) by an achromatic lens (Ø = 50 mm, f = 350 mm). The slit width for the present measurements was set to 75 μm. A front illuminated CCD camera (Andor Technology DV401-FI) is used as a detection device.

As a result of the intrinsic weakness of linear Raman scattering the scattered photons are collected over a period of 600 s from a continuous jet expansion. For each sample spectrum a background spectrum is recorded to reduce baseline artifacts. Artifacts from cosmic rays that dominate the raw spectra are removed by comparison of equivalent measurements. The spectra presented in this work are averages over 10 measurements. The expansion is probed only 1 mm away from the nozzle, which is one of the reasons why Ar relaxation and Ar nanocoating experiments do not work well in this case. Therefore, only Raman spectra from expansions in He are reported. While the rotational temperature of the monomers ($\approx$50 K) and dimers appears to have dropped to fairly low values after such a short expansion, the vibrational and conformational temperatures are most likely higher than in the IR case.

n-Alkanol Structure, Ar Coating, and Dimerization

J. Phys. Chem. A, Vol. 111, No. 31, 2007 **7439**

1-Propanol (≥99.8%, Merck), 1-butanol (≥99%, Acros), 1-pentanol (99%, Acros), 1-hexanol (Merck), helium (99.996%, Air Liquide), and argon (99.998%, Air Liquide) were used as supplied.

Monomer energies and harmonic vibrational frequencies were calculated using the Gaussian 03 program,[37] employing the standard 6-311+G* basis set, unless indicated otherwise. B3LYP and MP2 geometry optimizations and harmonic force field calculations (up to MP2/aug-cc-pvtz for propanol) as well as MP2 and occasional CCSD(T) energy calculations are reported. For selected butanol conformations, MP2 single point calculations involving the aug-cc-pvtz and aug-cc-pvqz basis sets were added to investigate basis set sensitivity at the correlated level. They are denoted MP2/av*xz*-sp with *x* = t, q. Selected dimer calculations have also been carried out. These calculations are only meant to explore the experimentally investigated properties and will have to be augmented considerably in future work, as an accurate description of subtle bonding and dynamics effects cannot be expected at such levels. Anharmonic perturbation theory was applied to the ethanol dimer[15] but resulted in a more or less uniform shift of the OH stretching frequencies. For a direct comparison of theory and experiment, experimental anharmonicities would be desirable. Overtone transitions are too weak in dimers to be useful in this context, but OD stretching fundamentals have been used successfully in the case of methanol and its clusters.[38]

For a crude initial modeling of the donor OH stretching absorptions in *n*-alkanol dimers, we start from a recently proposed,[14] simplified force field for aliphatic alcohols. This force field is based on a standard (parm99) AMBER set of intramolecular harmonic bond and intermolecular Lennard-Jones parameters,[39] which are augmented by partial charges of +0.42 *e* on the OH hydrogen and −0.71 *e* on the oxygen. The adjacent C atom accounts for electroneutrality, whereas all other atoms remain uncharged. The harmonic OH stretching frequency in such a simple force field is not sensitive to the OH conformation relative to the alkyl chain, but it reproduces the donor red-shift upon dimerization for a wide range of alcohol dimers.[14] Therefore, the dimer OH donor spectrum is simulated by convoluting the experimental monomer spectrum with a distribution of dimer frequencies obtained from a large set of dimer geometry optimizations based on randomized starting structures. For this purpose, the potential energy surface is scanned with a module of the TINKER[40] suite of programs using the parm99.dat force field. Conformational searches based on a basin hopping method are performed with different starting structures. The number of minima located on the potential energy hypersurfaces (PES) grows from about 20 for ethanol dimer to about 80 000 for the hexanol dimer. Using the AMBER8[41] suite of programs and in particular the NMODE module, the resulting structures are characterized with respect to the donor OH normal mode.

A histogram of OH stretching frequencies is collected for each alcohol. Subsequently, the dimer histogram is shifted by the predicted red-shift for the most stable dimer structure relative to the experimental monomer wavenumber (124 cm^{-1}, independent of the chain length). As monomer spectral intensities and band widths depend on the expansion conditions, they are adopted from experiment. A simple and uniform five-point band profile is used for all monomer bands. The integrated dimer-to-monomer intensity ratio is also adopted from the experimental spectra. However, the relative dimer abundances are chosen equal for each class of donor conformations observed in the monomer spectra, as the case of ethanol dimer[15] has revealed
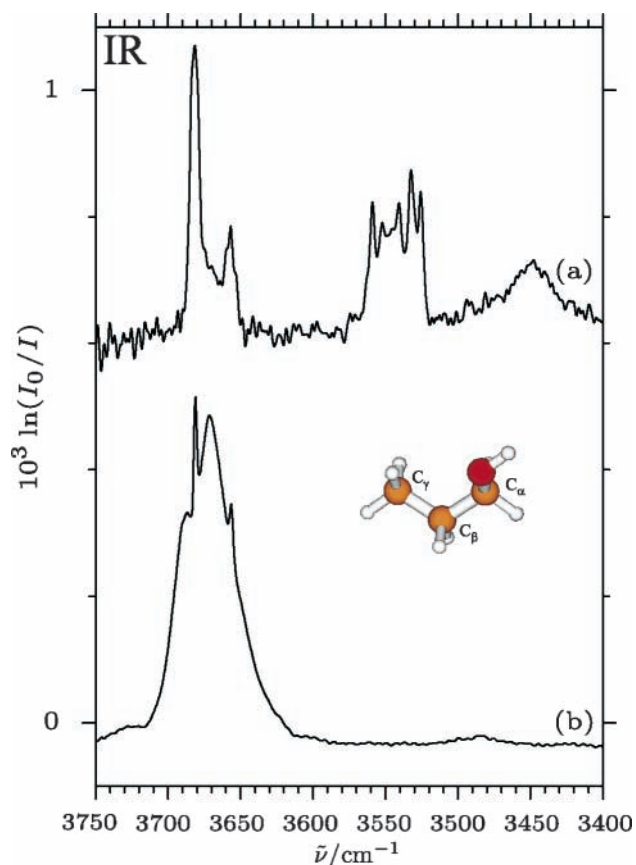

Figure 1. Supersonic jet (trace a, 500 scans), 0.07% in He, 0.75 bar stagnation pressure, and gas phase (trace b, scaled by 1/30) IR spectra of propanol together with the G+t conformation.

extensive redistribution of monomer conformations within the dimer, for which a prediction would be difficult.

3. Monomer Results

3.1. Propanol. Figure 1 compares the IR spectrum of propanol in the gas phase with that obtained in a supersonic jet expansion in the OH stretching region. The latter is in good agreement with an earlier measurement[9] using the first generation of pulsed high-throughput nozzle FTIR spectroscopy. The rotational substructure in the gas-phase reveals at least two conformers, as evidenced by the sharp Q-branches. While the higher-frequency peak (3682 cm^{-1}) dominates, the lower frequency contribution (3657 cm^{-1}) is also substantial but difficult to quantify. This is easier in the supersonic jet expansion (upper trace), where the P and R branches merge with the Q-branch transitions at the employed spectral resolution. The $T^{1/2}$ dependence of the rotational profile indicates a rotational temperature close to 10 K. A series of overlapping dimer absorptions and a broad trimer absorption are seen around 3550 and 3450 cm^{-1}, respectively. The high-frequency monomer peak is now even more dominant, already indicating that it arises from more stable conformations than the lower-frequency peak.

Propanol has 3^2 rotamers, all with rotational symmetry number 1 (for a diverging view, see ref 29), which can be interconverted by torsions around the C$_\alpha$−O (t, g+, g−) and C$_\beta$−C$_\alpha$ (T, G+, G−) bonds. The all-trans (Tt) conformation has a mirror plane, whereas the other eight conformations come in enantiomeric pairs, which are not distinguishable in the present experiments. Their statistical abundance has to be doubled, if they are not considered as separate systems. The + (−) sign is used for a synclinal or gauche conformation, if it is

7440 *J. Phys. Chem. A, Vol. 111, No. 31, 2007*

Wassermann et al.

TABLE 1: Energy Differences in kJ/mol between the Global Minimum (G+t) Conformation of Propanol and Higher Energy Local Minima (in Parentheses Including Harmonic Zero Point Energy)

conformation	B3LYP	MP2	MP2-sp	MP2/avtz	CCSD(T)[a]
Tt	0.1	1.7	1.5	0.7 (0.5)	0.3
Tg	0.3	1.7	1.6	1.1 (1.0)	0.5
G+g+	0.9	1.3	1.2	1.0 (1.0)	0.5
G+g−	1.2	1.9	1.8	1.1 (1.2)	0.6

[a] Basis set extrapolation.[33]

TABLE 2: OH Wavenumber Differences in cm^{-1} between Local Minima and the Global Minimum (G+t) Conformation of Propanol

conformation	B3LYP	3P[a]	MP2	MP2/avtz
Tt	−5	−5	−3	−2
Tg	−20	−20	−11	−11
G+g+	−22	−20	−15	−15
G+g−	−6	−5	+3	−3

[a] 3P is a simple three-parameter model designed to fit the B3LYP predictions for several *n*-alkanols.

obtained from the synperiplanar or cis conformation by ≈60° clockwise (anticlockwise) rotation of the distant segment around the torsional bond. Alternatively, the direction of the rotation is indicated by the use of primes (g, g′).[29] Note that the nomenclature is not always used in this way.[24,33,42] In summary, Tt, Tg−/Tg+ = Tg, G+t/G−t = Gt, G+g+/G−g− = Gg$_{hom}$, and G+g−/G−g+ = Gg$_{het}$ could give rise to five distinguishable OH stretching absorptions. We use the abbreviation Gg$_{hom}$ (Gg$_{het}$), where emphasis is on the relative configuration or conformation of the two adjacent torsional angles. While conformation is at the focus of the present work, the relative configuration or helicity of the torsional segments can be of interest in chiral recognition studies.[43] Unspecified conformations around the C$_\alpha$−O and C$_\beta$−C$_\alpha$ bonds will be denoted x and X, respectively. According to quantum chemical calculations, there appears to be a systematic increase in IR (by ≈ 10−40%) and even more so in Raman activity (by about a factor of 2) when moving from gauche to trans OH groups. Therefore, trans conformers are somewhat more visible in the following IR and Raman spectra.

Exploratory geometry optimizations at the B3LYP and MP2 levels using the 6-311+G* basis set provide the following energetic picture for these five conformers (only the first of the enantiomers listed above will be subsequently used): G+t is the most stable structure (shown in Figure 1), and the other four are up to 1.2 (B3LYP) or 1.9 kJ/mol (MP2) higher in energy. Single point MP2 calculations at the B3LYP minimum structures (MP2-sp) deviate by less than 0.2 kJ/mol in relative energy from fully optimized MP2 structures, which is encouraging for the calculation of longer chain alcohols. A geometry optimization at the MP2/avtz level conserves the global minimum property of the G+t structure. However, the detailed energetical sequence is not systematic among the B3LYP and MP2 calculations (see Table 1). Increasing the basis set within the B3LYP approach does not solve the problem, either.[42] Not surprisingly, the comparison to a recent high-level analysis involving basis set extrapolations and corrections up to CCSD-(T) level[33] confirms that such approaches are far from converged in terms of the relative energies. Please note that for the Tt conformation, we use the energy value given in the text rather than the one in Table 7 of ref 33. Furthermore, partial zero-point energy corrections[33] have not been included for consistency. However, it appears that the MP2/avtz approach, while overestimating relative energy differences by about a factor of 2, provides a good compromise between accuracy and computational effort. In this case, the harmonic zero point energy effects have also been evaluated and are given in parentheses in Table 1. They only have a minor influence on the conformational sequence.

Recent MW work[29] indicates that the experimental energy differences between the different conformations of *n*-propanol may be even smaller than predicted by high level quantum calculations. Energy differences below 1 kJ/mol still pose a serious challenge to theory for molecules of this size and may

even change sign upon inclusion of anharmonic zero point energy, in particular considering large amplitude motion along the coupled torsional degrees of freedom. Nevertheless, it should be noted that at all levels considered in Table 1, the Gt conformation is found to be the global minimum structure. This structure has recently been studied in detail by rotational spectroscopy.[29]

On the other hand, numerous earlier experimental (refs 20 and 30 and references cited therein) and theoretical[20,23,44] studies have identified other conformations to represent the global minimum of *n*-propanol. Therefore, the exact zero-point corrected energy sequence of the *n*-propanol conformations, which is among the most delicate we know for such simple molecules, must still be considered to be uncertain at this stage.

In contrast to the energy sequence, the OH stretching wavenumbers behave more regularly in our exploratory quantum chemical calculations. Table 2 summarizes some harmonic predictions relative to the OH stretching wavenumber of the G+t conformation.

The presumably most stable G+t conformation is consistently predicted to have the highest OH stretching frequency, together with the Tt conformation and (note the typographical error in Table 3 of ref 23) the least stable G+g− conformation. A local mode treatment[42] suggests that the Tt form may have a higher transition wavenumber than the Gt form, whereas the harmonic calculations in this and other work[23] predict a closer match between the two. The other two conformers, which contain a gauche OH conformation, are predicted to absorb at significantly lower wavenumber. This bunching of the OH stretching absorptions into two groups is in good agreement with the jet FTIR spectrum (Figure 1), although the experimental t/g shift of −25 cm^{-1} is underestimated by the harmonic calculations, in particular at the MP2 level. A possible explanation for the special position of the G+g− OH stretching band is the short distance between the hydroxyl H and a terminal methyl hydrogen (B3LYP, 2.37 Å; MP2, 2.32 Å; MP2/avtz, 2.24 Å; see also Figure 5 below). In the absence of such higher-order interactions, t-configured isomers appear to be more stable and higher in OH stretching frequency than g-configured isomers, in nice agreement with the double-peak structure of the jet-FTIR spectrum and the findings for ethanol.[15]

If one wants to go beyond such a coarse-grained analysis, significantly higher levels of theory and better resolved experimental spectra are required. An elegant way to achieve the latter is to switch to Raman spectroscopy. While the band centers should remain the same, the Raman selection rules emphasize the sharp Q-branches over the broader $\Delta J \neq 0$ branches. This is already the case for the room-temperature gas-phase spectrum of propanol, which is shown in the lower trace of Figure 2. It compares favorably to an early, less structured gas-phase spectrum recorded at higher pressure and temperature.[45] Between two bands at 3683 cm^{-1} and 3657 cm^{-1} which are in good agreement with the IR spectra, an additional band is visible at 3669 cm^{-1}. The jet spectrum in the upper trace confirms the

n-Alkanol Structure, Ar Coating, and Dimerization

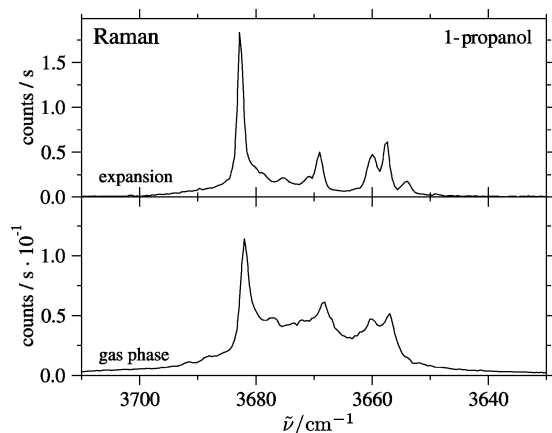*J. Phys. Chem. A, Vol. 111, No. 31, 2007* **7441**

Figure 2. Supersonic jet (0.5% in He, 1 bar stagnation pressure) and gas-phase Raman spectra of propanol.

existence of this monomer band and provides a better background suppression. The jet spectrum reveals that the low-frequency band actually consists of three peaks at 3660 cm^{-1}, 3657 cm^{-1}, and 3654 cm^{-1}. In hindsight, this substructure and the additional band near the center may also be found in the IR spectrum (Figure 1), but the jet Raman profile is far more conclusive and better resolved. Although the collapse of rotational structure from the gas phase to the jet may account for some intensity effects, the 3683 cm^{-1} band clearly profits from cooling and must be associated with more stable conformations.

On the basis of the exploratory calculations in Table 2, possible candidates for the 3669 cm^{-1} band are the Tt or the G+g− conformation. The former interpretation is somewhat more likely, as we will see below. The three bands around 3657 cm^{-1} may be due to three different conformations, but a tunneling splitting due to OH internal rotation in particular for Tg[29,30] and a dimer origin of the lowest frequency band should not be ruled out.

To corroborate the conformational energy sequence, Ar relaxation experiments were carried out in the IR study. In these experiments, the admixture of increasing amounts of Ar to the He carrier gas promotes relaxation from local minima into the global minimum structure. It is fairly well-established that isomerization barriers on the order of several kJ/mol can be easily surmounted in this way.[15,46] Unfortunately, the limited sensitivity of the Raman experiment does not allow for the probing of sufficiently large nozzle distances. At 1 mm away from the nozzle, the effects are too weak to be observed. However, IR spectra at a nozzle distance of 10 mm do show substantial relaxation effects, as illustrated in Figure 3. The addition of 1−4% Ar (traces b and c) is enough to substantially deplete the g isomer population, which gives rise to the low-frequency OH stretching modes. Higher Ar concentrations lead to nanocoating and will be discussed below. The relaxation effect strongly confirms that stability correlates positively with high OH stretching frequency, as indicated before. The band around 3669 cm^{-1} appears to better survive the relaxation process. A straightforward interpretation would be that propanol prefers a t-configured OH group, much like ethanol.[15] The additional methyl group appears to favor a G conformation, which offers the possibility for a weakly attractive interaction with an oxygen lone pair. However, an all trans, stretched conformation seems to exist as well in minor quantities and to survive the relaxation experiment. Clearly, this is a case which deserves further MW studies[29] and detailed ab initio analysis,
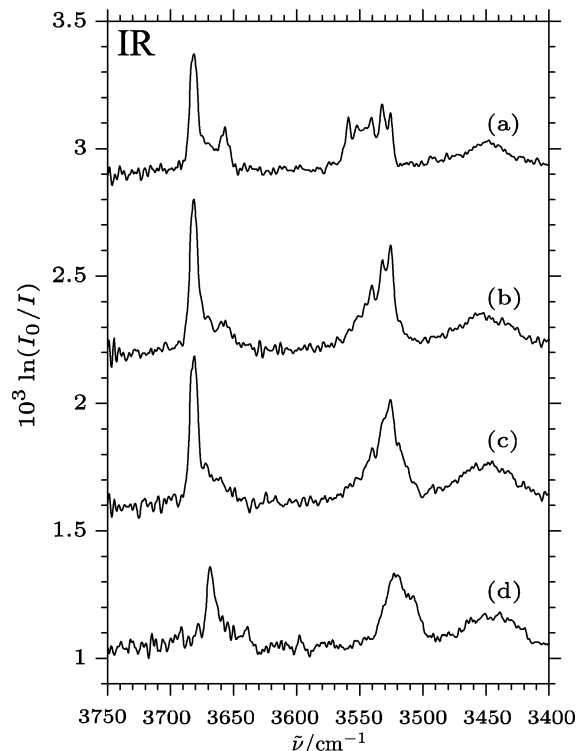

Figure 3. Argon relaxation study for 0.07% propanol in He expansions (150−500 scans each) at 0.75 bar stagnation pressure: (a) 0% Ar, (b) 1% Ar, (c) 4% Ar, and (d) 0.05% propanol in pure Ar.

but a tentative spectral and stability sequence based on our experimental data is Gt > Tt > several g conformations.

Next, we want to discuss the expansion in pure Ar (trace d in Figure 3). Here, the dominant OH stretching band of free propanol at 3681.5 cm^{-1} has disappeared almost completely. Instead, a new band at 3669 cm^{-1} appears. The overlap with the secondary isomer shoulder of free propanol around 3669 cm^{-1} is coincidental. Rather, comparison to similar observations for HCl,[9] methanol,[35] ethanol,[15] pyrazole,[11] and several other examples suggests that this new band corresponds to Ar-coated propanol, that is, propanol molecules which are embedded in a probably amorphous Ar nanomatrix. A shift of −12.5 cm^{-1} is typical for an Ar matrix environment. Indeed, the highest frequency absorption band of propanol embedded in a crystalline Ar matrix[20,23] is at 3665 cm^{-1}. The small difference may be explained by the lack of crystallinity and by the finite size of the Ar coating, which may not even involve the entire molecular surface. The bulk Ar matrix spectrum has been analyzed in terms of up to five spectral contributions due to different conformers,[23] which are spread by only 8 cm^{-1}. Although the Ar perturbation is on the same order of magnitude as this isomer spread, an assignment to individual conformers was attempted.[23] It is based on the assumption that the (theoretically predicted) room-temperature equilibrium distribution is frozen upon matrix deposition. The overestimated population of the Tt conformer[23] indicates that the energy of this conformation should be higher than predicted.[23] Indeed this is the case in our exploratory calculations as well as in the high level basis set extrapolations.[33] The reduced frequency spread of the matrix-embedded conformers may be explained by a stronger interaction of t conformations with the matrix, compared to the more protected g position of the OH group. In the matrix investigation, further evidence for a t preference of the high-frequency components was obtained based on the analysis of C$_\alpha$−D stretching modes. Under certain conditions, the latter were shown to be very
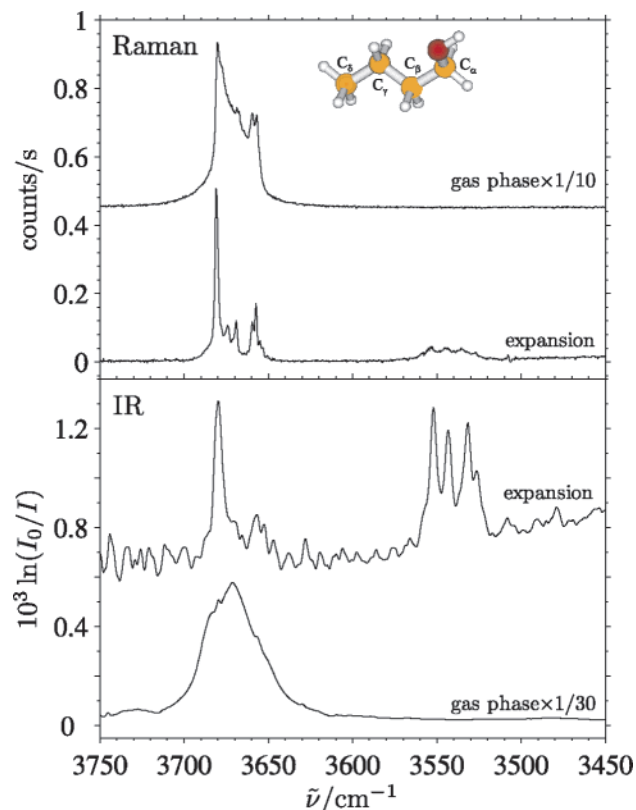
Figure 4. *n*-Butanol Raman (0.27% butanol in He) and IR spectra (0.06% butanol in He) in supersonic jet expansions and in the gas phase together with the structure of the TG+t conformation.

TABLE 3: Energy Differences in kJ/mol between the Global Minimum (TG+t) Conformation of Butanol and Local Minima

conformation	B3LYP	MP2	MP2-sp	MP2/avtz-sp[a]	MP2/avqz-sp[b]
TTt	0.5	2.4	2.2	1.0	1.0
TTg	0.7	2.3	2.1	1.4	1.4
TG+g+	1.0	1.5	1.4	1.1	1.2
TG+g−	1.4	2.0	1.9	1.2	1.2
G+G+t	3.2	1.0	1.6	1.1	1.3
G+G+g+	3.7	2.3	2.7	2.2	2.3
others	>4	≥4	>4		

[a] MP2/aug-cc-pvtz energy at MP2/6-311+G* geometry. [b] MP2/aug-cc-pvqz energy at MP2/6-311+G* geometry.

sensitive probes of the OH conformation.[23] Thus, there is strong evidence from the combined free jet, bulk, and nanomatrix experiments that the higher frequency component of the OH stretching mode arises from a t conformation, both in isolated and in embedded propanol. The relaxation experiment as well as the jet cooling effect support the theoretical prediction that this is also the most stable OH group arrangement. Evidence for the preference of a G conformation around the C−C bond is more indirect and rests on subtle but systematic theoretical predictions on its stability and relative OH stretching frequency. Here, MW experiments[29] or vibrational studies in the more characteristic fingerprint range appear indispensable to provide a definitive answer.

3.2. Butanol. One way in which we can further contribute to an understanding of this subtle isomer equilibrium in 1-propanol is by studying homologous compounds. Therefore, we discuss 1-butanol as the next example. The IR and Raman spectra are shown in Figure 4. While the IR gas-phase spectrum weakly indicates the presence of more than one isomer, the jet-IR spectrum clearly reveals that this is the case and that the higher frequency OH stretching band again corresponds to the most stable conformers. The Raman jet spectrum contains more detailed information as a result of the sharpness of the Q branches. Again, at least four bands within 2 cm^{-1} of the corresponding 1-propanol bands can be attributed to monomers, whereas the small peak at 3674 cm^{-1} is more likely due to a dimer OH acceptor mode.

The close analogy between propanol and butanol suggests a common assignment of all bands. An exploratory investigation of all 14 distinguishable conformations at B3LYP and MP2 level reveals some robust energetical features, which are summarized in Table 3. In all cases, the TG+t conformation is the most stable. It can be derived from the most stable propanol

conformation by adding the new methyl group (C$_\delta$) trans to the C$_\beta$−C$_\alpha$ bond.

At the B3LYP level, this is also true for the next four low-energy structures, whereas the MP2 calculations predict an unusually stable G+G+t structure below most of the other TXx conformations. To explore the effects of basis set size, energy calculations at the optimized MP2/6-311+G* structures were carried out using the large avtz and avqz basis sets. There is very little basis set dependence in this range for the most stable conformations, as seen in the table. This suggests that basis set effects beyond the avtz basis for MP2 calculations are small compared to structural relaxation, (an)harmonic zero point energy corrections, and higher correlation effects. None of these effects is likely to overturn the global stability of the TGt conformations. Nevertheless, systematic higher level calculations will definitely be required in this field to differentiate among the local minima. Exploratory CCSD(T) calculations indicate that the relevant energy differences decrease upon inclusion of electron correlation beyond the MP2 level. Also, it will be interesting to explore the reason for the persistent stability of the G+G+t conformation, which may be related to weak attraction between the ends of the molecular chain.

Our energetical findings are in qualitative agreement with recent anharmonically corrected *n*-butanol calculations at the B3LYP/6-31++G(d,p) level of the TXx conformations only.[24] Again, the TGt conformation is found to be the most stable, closely followed by the TTt conformation. Butanol is the smallest *n*-alkanol which can also occur in sterically hindered conformations, namely, G+G−x. They are unlikely to be abundant in the supersonic jet expansion and have not even been observed in condensed phase spectra.[21]

The wavenumber pattern predicted for the most stable conformations at the B3LYP and MP2 levels is given in Table 4. It follows the one predicted for propanol quite closely, which is again consistent with our experimental observation of closely similar spectra. The overall spread of the experimental OH stretching wavenumbers for the different conformations is about 26 cm^{-1}. Like in the case of propanol, the B3LYP predictions capture this spread better than the low level MP2 results. In this context, however, the anharmonic B3LYP calculations in ref 24 show a marked difference. They predict a wavenumber shift of +10 cm^{-1} for the TTt conformation, which appears to contradict our experimental stability−wavenumber correlation.

On the basis of the semiquantitatively reliable and computationally scalable harmonic B3LYP wavenumber results, it is tempting to develop a simplified model for the relative OH stretching wavenumbers in the different monomer conformations, which can subsequently be used to identify unusual conformations. We propose a basic three-parameter model (3P), which assumes that a change from t to g generally lowers the

n-Alkanol Structure, Ar Coating, and Dimerization

J. Phys. Chem. A, Vol. 111, No. 31, 2007 **7443**

TABLE 4: OH Wavenumber Differences in cm⁻¹ between the Global Minimum (TG+t) Conformation of Butanol and the Six Lowest Local Minima[a]

conformation	B3LYP	3P	MP2
TTt	−7	−5	−2
TTg	−20	−20	−9
TG+g+	−22	−20	−12
TG+g−	−4	−5	+6
G+G+t	0	0	
G+G+g+	−22	−20	
G+Tt	−5	−5	
G+Tg+	−20	−20	
G+Tg−	−22	−20	
G+G+g−	−9	−5	
G+G−t	−5	0	
G+G−g−	−18	−20	
G+G−g+	+9	(−5)	

[a] Below the separation, predictions for the higher energy structures are also shown to develop a simplified model.

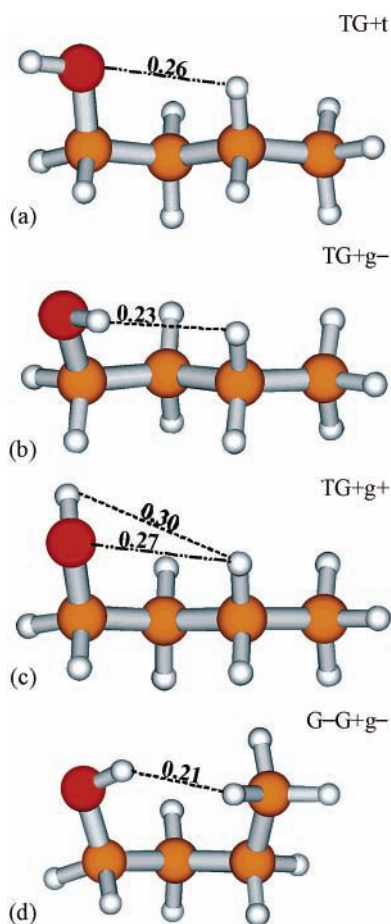**Figure 5.** Geometrical rationalizations for the 3P model parameters. (a) CH···lone electron pair interaction in Gt alkanols exemplified for TG+t, (b) OH···H proximity in G+g−/G−g+ configured alkanols (Δṽ = +15 cm⁻¹), (c) OH···H distance and CH···lone electron pair distance for G+g+/G−g−, (d) CH₃···HO proximity in G+G−g+ or G−G+g− butanol as a higher order effect. Distances (nm) calculated at the B3LYP/6-311+G* level.

wavenumber by about 20 cm⁻¹ but allows for two higher order corrections: A G+g− conflict raises the wavenumber by 15 cm⁻¹ and the absence of a Gt pairing in a t conformation lowers it by 5 cm⁻¹. Both corrections can be justified by nonbonded interactions (see Figure 5).

In a G+g− or G−g+ sequence, the hydroxyl hydrogen approaches the C_γ hydrogen quite closely and leads to repulsion, whereas this contact is avoided in a G+g+ sequence. We note

that such repulsive contacts can be turned into attractive ones with concomitant wavenumber reduction by partial fluorination.[43]

In a Gt pairing, one of the oxygen lone pairs comes close to a C_γ hydrogen, which appears to raise the OH stretching wavenumber somewhat. The absence of such an interaction in a t-configured OH group (e.g., in ethanol) thus lowers the wavenumber.

For ethanol, the model predicts a t/g splitting of 20−5 cm⁻¹, equal to the B3LYP value of 15 cm⁻¹. For propanol and butanol, the model predictions are listed in Tables 2 and 4 and lead to a 30% larger spread in wavenumber among the most stable conformations than in ethanol.

An equivalent, less physical formulation of the 3P model for the OH stretching wavenumber shift $\Delta\tilde{\nu}_{OH}$ relative to the most stable Gt arrangement of $C_\gamma C_\beta C_\alpha$ OH would be

$$\Delta\tilde{\nu}_{OH}/cm^{-1} = -15\delta(x-g) + 5\delta(X-G) - 5\delta(Xx - Gg_{hom}) + 10\delta(Xx - Gg_{het}) - 5$$

Here, Gg_{hom} (Gg_{het}) stands for a G+g+ or G−g− homoconfigurational (G+g− or G−g+ heteroconfigurational) neighborhood and $\delta(a-b)$ equals 1 if $a = b$, and 0 elsewhere.

With one exception, the model reproduces the calculated ethanol, propanol, and butanol wavenumber shifts quite well. More than 80% of the differences are smaller than 3 cm⁻¹. Only the G+G−g+ butanol prediction deviates by more than 5 cm⁻¹, but this is easily understood. In the G+G−g+ arrangement, the G−g+ conflict between the hydroxyl hydrogen and the C_γ hydrogen is aggravated, as the latter is now replaced by a C_δ group. This causes a further rise of the OH stretching wavenumber. It will not be easy to verify this experimentally, as the G+G−g+ conformation is predicted to be the least stable of the 14 butanol structures. However, the success of such a simple model for the harmonic B3LYP OH stretching frequencies raises hope for a future similar model describing the experimental stretching fundamentals. Ultimately, it will of course be more satisfactory to model the force field rather than the frequencies.[26]

Ar relaxation experiments for butanol jet expansions show very similar effects as in the case of propanol. The most redshifted OH stretching bands disappear, whereas the dominant high-frequency band and also the much weaker intermediate wavenumber band persist.

3.3. Longer Chains and Chain Length Trends. Similar IR and Raman studies were carried out for 1-pentanol and 1-hexanol. The observed band maxima are summarized in Table 5, together with those of the shorter homologs. While the signal-to-noise ratio deteriorates and IR interference by atmospheric water traces aggravates, the observed pattern is the same, with a dominant high-frequency monomer transition, a much weaker band shifted to lower frequency which persists upon Ar relaxation, and a cluster of low-frequency bands which tends to disappear upon Ar relaxation. The invariance of the intermediate transition points at a common XTt assignment (although sterically hindered Xg conformations cannot be ruled out), whereas the strongest band is probably dominated by XGt conformations and the low-frequency signals arise from Xg conformations which do not have unfavorable C_γ−hydroxyl interactions. The dominance of the high-frequency monomer band was recently confirmed for *n*-octanol.[14]

In Table 6 some model predictions for selected pentanol conformations are also shown. The conformations were obtained from the 14 butanol conformations by addition of a CH₃ group with T configuration at the carbon chain end. Again, and not

TABLE 5: Experimental IR and Raman Band Maxima ṽ in cm⁻¹ (IR/Raman), for Ethanol, Propanol, Butanol, Pentanol, and Hexanol Monomers and Dimers

(a) Monomers					
Ethanol					
3678[15]/3677[36]	−/3671[a]		3661[15]/3659[36]		−/3654[a]
1-Propanol					
3682/3683	−/3675[a]	3670/3669	−/3660	3657/3657	−/3654[a]
1-Butanol					
3680/3681	−/3674[a]	3670/3669	−/3659	3657/3657	−/3655[a]
1-Pentanol					
3680/3681	−/3674[a]	3668/3668	(3659)/3659	3656/3657	
1-Hexanol					
3680/3681	−/(3672)[a]	3671/3668	−/3659	3658/3657	
(b) Dimers					
Ethanol					
	3547[15]/3548[36]	3540[15]/3541[36]	3532[15]/3532[36]		
1-Propanol					
3559/3560	3552/3551	3541/3542	3532/3534	3526/3527	
1-Butanol					
−/3559	3552/3553	3543/3544	3532/~3535	3526/~3528	
	3552.0[10]	3543.5[10]	3532.8[10]		
1-Pentanol					
3557/3557	3551/3553	3544/3545		3527/3528	
1-Hexanol					
	3552/3553	3546/3546	3538/~3535	3526/~3528	

[a] Possibly dimer acceptor peaks.

TABLE 6: OH Wavenumber Differences in cm⁻¹ between the Lowest Energy TXXx Conformation of Pentanol (TTG+t) and the 13 Other TXXx Conformations Corresponding to the Butanol Conformations (Table 4)[a]

conformation	B3LYP	3P	conformation	B3LYP	3P
TTTt	−6	−5	TG+Tt	−5	−5
TTTg	−19	−20	TG+Tg+	−19	−20
TTG+g+	−21	−20	TG+G+g−	−8	−5
TTG+g−	−3	−5	TG+G−t	−4	0
TG+G+t	1	0	TG+G−g−	−16	−20
TG+G+g+	−21	−20	TG+G−g+	+4	(−5)
TG+Tg−	−21	−20			

[a] Conformations are ordered by increasing B3LYP energy.

TABLE 7: Dominant OH Stretching Band Maxima in cm⁻¹ for n-Alcohol Monomers in Pure He Expansions (He) and Wavenumber Shifts Observed in Ar Expansions (Ar Coated) as Well as Matrix Isolation (Ar-Matrix)

alcohol	He	Ar-coated	Ar-matrix
ethanol	3678[15]	−17[15]	−17, −22[16]
propanol	3681.5	−12.5	−17[23]
butanol	3679.8	−13.2	−10, −17[21]
pentanol	3679.6	−12.1	
hexanol	3679.5	−13.5	

surprisingly, the model is found to perform well in reproducing the B3LYP results, with the exception of the sterically hindered TG+G−g+ conformation, which is energetically unfavorable. The even more unfavorable G−G+G−g+ conformation collapses into another conformation upon structure optimization. The G−G+G+g− conformation, which also involves sterical hindrance, is predicted at −13 cm⁻¹, far away from the model prediction of −5 cm⁻¹.

For co-expansions with high Ar concentrations up to pure Ar, a dominant, somewhat broader monomer band persists in all investigated alcohols (Figures 3, 7, and 8). It is characteristically red-shifted with respect to the isolated XGt monomer band. Like in the case of ethanol,[15] it is due to alcohol molecules which are more or less completely coated with Ar atoms. The shift is quite discontinuous and not very sensitive to the detailed conditions. Table 7 lists the observed band maxima and shifts. There is a subtle but systematic alternation in the Ar-nanomatrix induced red-shift with alkyl chain length. Alcohols with an odd number of carbon atoms are perturbed less strongly by the solvating Ar atoms than alcohols with an even number of C atoms. It will be a challenging task for molecular modeling approaches[47] to describe this subtle packing effect, which occurs despite several indications that the Ar atoms do not form a rigid crystalline matrix for the molecules, as they do in bulk matrices.

It will also be interesting to investigate whether bulk matrices show similar or even larger alternation effects or whether the alternation is masked by site splittings due to the crystalline nature of the matrix.

Alternation effects in n-alkanols are abundant in their crystalline state. For long chain alcohols, it is known[13] that even-membered alkyl groups lead to all-trans monomers, whereas odd-membered alkyl groups favor alternating chains of G and T conformations for the C−C−C−O torsional angle. Even in the evaporation process, there are residual odd−even alternations.[48] Even-membered chain alcohols have relatively small enthalpies of vaporization and relatively large vapor pressures, at least at not too elevated temperatures. However, all this involves hydrogen-bonded alcohol molecules, which will be addressed in the next section.

4. Dimers

Having reached a semiquantitative understanding of the effects of conformational isomerism on the OH stretching spectra in alcohol monomers, we can turn our attention to hydrogen-bonded alcohol dimers. The donor OH bond is weakened by the hydrogen bond interaction and experiences a strong bathochromic shift, on the order of 120 cm⁻¹. The 3^{n-1} rotational isomers of $C_nH_{2n+1}OH$ can give rise to 3^{2n-2}

n-Alkanol Structure, Ar Coating, and Dimerization

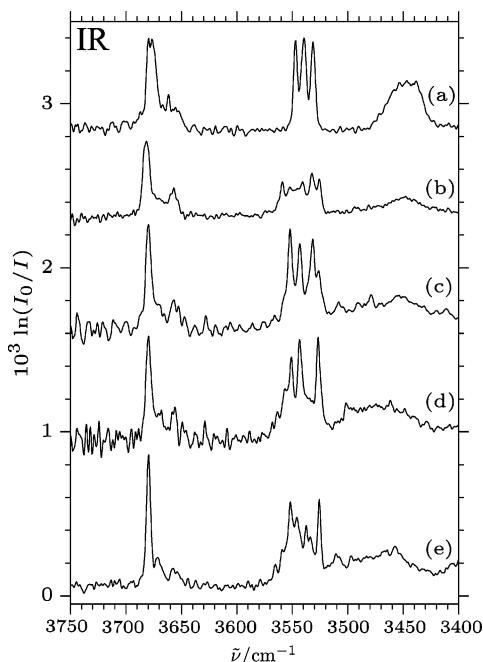*J. Phys. Chem. A, Vol. 111, No. 31, 2007* **7445**

Figure 6. Supersonic jet spectra of the *n*-alkanols ethanol through 1-hexanol in He. (a) 0.04% ethanol, ref 15, (b) 0.07% 1-propanol, (c) 0.06% 1-butanol, (d) 0.06% 1-pentanol, and (e) 0.02% 1-hexanol.

distinguishable dimer conformations, because there is a choice between two lone electron pairs at the acceptor oxygen, but for each dimer there is an indistinguishable mirror image. Not all dimers will be seen as separate absorption features in the jet spectrum. Given the width of the bands and the spread between gauche and trans transitions, extensive band overlap is expected. As in the case of monomers, one may expect to be able to differentiate between O—H and C$_\alpha$—O torsional isomers, at most. In the case of ethanol,[15] where up to nine dimers could have been expected in a simple rotational isomeric state analysis, only three bands, the center one indicative of band overlap, were observed.

Figure 6 summarizes the jet IR observations for the higher alkanols. The dimer donor bands are located between the monomer and the trimer absorptions as a fairly structured, narrow peak assembly. In the case of *n*-butanol, our spectrum is in very good agreement with an earlier cavity ring down study using a slit nozzle.[10] The overall bandwidth increases substantially from ethanol to propanol and slightly shrinks thereafter. This is consistent with C—C torsional isomerism beyond ethanol and with a narrowing of the number of distinguishable conformations with increasing chain length. Also, the number of dominant dimer bands tends to decrease from propanol (≥ 5) to hexanol (≥ 2).

Although we have carried out exploratory dimer calculations for propanol and butanol at B3LYP and MP2 levels, the detailed analysis for ethanol dimer has shown that it is very challenging for theoretical methods to closely reproduce the experimental findings.[15] Neither the spread of harmonic values nor the average red-shift is described well by the harmonic calulations at the B3LYP level using the 6-311+G* basis set. Perturbative inclusion of anharmonicity also does not remove the deficiencies.[15] Among the more robust properties was the observation that the most red-shifted ethanol dimer corresponds to the most stable one,[15] at least if the monomer stability sequence is taken into account.[49] Similar deficiencies in theoretical descriptions have recently been observed for *n*-butanol dimers.[24] Therefore, we refrain from presenting a selection of dimer calculations.

Instead, we can provide experimental constraints on stability−dynamics relationships in alcohol dimers.

In Figure 3, the effect of Ar relaxation (and coating) on the dimer intensity pattern is shown for propanol. Addition of 1% Ar clearly shows that the bands with the most pronounced red-shifts survive the relaxation. Therefore, they originate from the most stable dimer conformations. In analogy to the ethanol case,[15] it is tempting to assume that these involve gauche conformations for the OH group despite a trans preference in the monomer. Our exploratory calculations indicate that there is a large number of energetically competitive conformations. Their robust ordering with quantum−chemical methods will be very challenging and may stretch the limits of layered methods,[50] because dispersion interactions between the chains will compete with hydrogen bonding.

Already with 4% Ar added to the He, new dimer absorptions emerge further to the right. They are not due to dimer conformations which were unpopulated in the pure He coexpansion. Most likely, they represent the first signs of Ar nanocoating, which proceeds with increasing Ar concentration. The onset of Ar nanocoating occurs earlier in the dimer than in the monomer, as the former represents a more polarizable system which can also dissipate energy more efficiently. Furthermore, the enhanced dipole moment in most dimer conformations will promote Ar coating. In ethanol, it was possible to conclude from the small size of the dimer matrix shift that there is a conformational change from the free to the embedded dimer.[15,17] In the case of propanol dimers, there seem to be several conformations present in the matrix, but this requires further investigation, also in bulk matrices.[17]

Butanol, whose dimer region is more structured, shows a similar behavior upon Ar relaxation and coating. In an earlier IR-CRLAS investigation of butanol in a free jet expansion, three main dimer absorptions have been assigned to butanol dimers at 3532.8, 3543.5, and 3552.0 cm^{-1}.[10] This corresponds well to our measured band positions of 3532, 3543, and 3552 cm^{-1}. A small shoulder at the low-frequency side at 3526 cm^{-1} was also visible in the IR-CRLAS spectra, though not further mentioned in the text. Our Ar relaxation experiments provide new information about the energetic succession of the species underlying the mentioned absorptions. Again, like in the propanol case, the most red-shifted dimers survive the relaxation best and may be linked to the most stable dimer structures. Weak indications of coating effects can already be found upon the addition of 2.5% Ar to the carrier gas.

For pentanol, the pattern is somewhat different (Figure 7). Here, two out of the three prominent dimer peaks appear to survive Ar relaxation, and it is not clear which one belongs to the most stable dimer. However, the most blue-shifted peaks drop in intensity and certainly do not represent the most stable dimers. The first signs of Ar coating are noticeable upon the addition of 2% Ar to the carrier gas (Figure 7, trace c). In this context, one should note that the crystal structure of 1-pentanol is built exclusively from g-configured units.[22] Thus, there is a complete change of conformational preference from the gas phase to the solid, and the most stable conformation of the dimer would be of particular interest.

Finally, the hexanol spectra do not show a clear relaxation pattern any more. Signs of Ar nanocoating are already observed in a spectrum containing only 1% Ar in the carrier gas (Figure 8, trace b). The structure of the dimer peak compared to the He expansion spectrum (trace a) has changed completely, and the whole band is slightly shifted to the red. Apparently, several of the many (theoretically 3^{10}) possible dimer structures are too
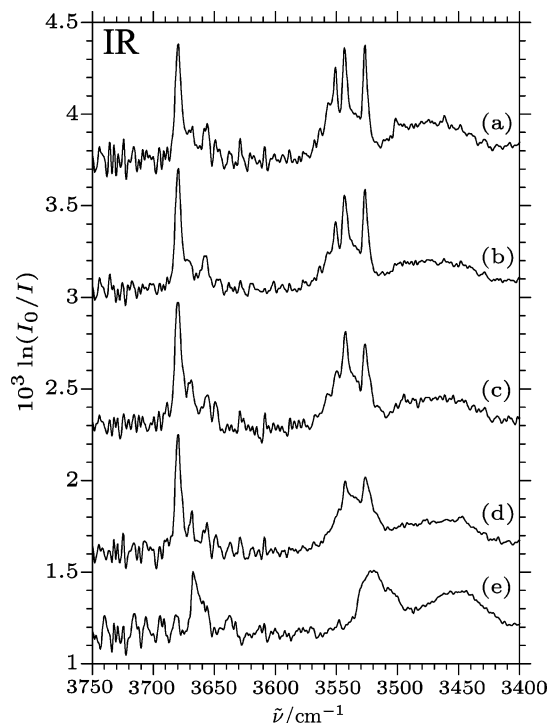
Figure 7. Argon relaxation study for 0.06−0.1% pentanol in He expansions at 0.5−0.75 bar stagnation pressure. (a) 0% Ar, (b) 1% Ar, (c) 2% Ar, (d) 5% Ar, and (e) 0.06% pentanol in pure Ar.
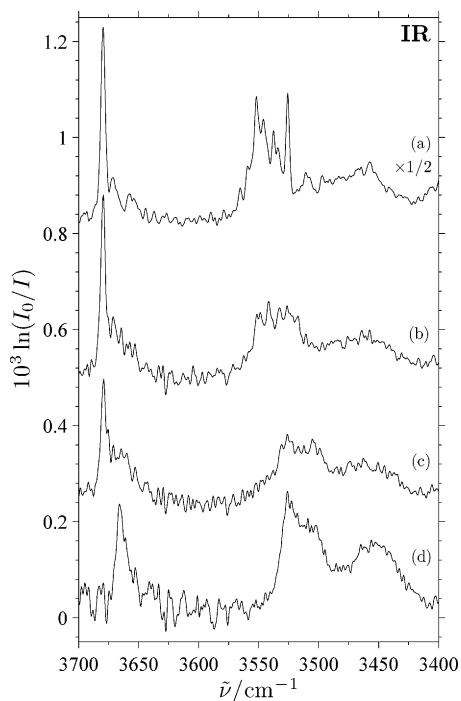

Figure 8. Argon relaxation study for ≈0.02% hexanol in He expansions at 0.8−1.5 bar stagnation pressure. (a) 0% Ar, (b) 1% Ar, (c) 5% Ar, and (d) 0.04% hexanol in pure Ar.
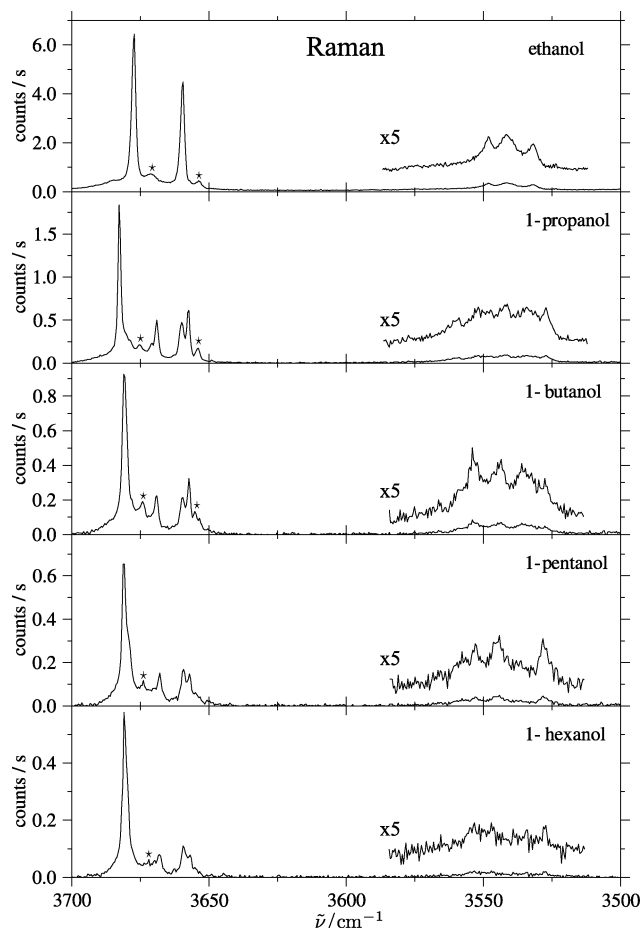

Figure 9. Raman jet spectra of the *n*-alkanol monomers and dimers in the OH stretching region. The asterisks mark transitions in the monomer region which are likely to be due to dimer acceptor bands.

similar in energy or too well separated by barriers for efficient relaxation. Therefore, we observe a stepwise coating effect, evidenced by a progressive increase of the shift of the overall dimer band with addition of Ar to the carrier gas. The same seems to apply for the monomers at higher Ar concentrations. A spectrum of 5% Ar already shows weak indications of nanocoating (Figure 8, trace c). In this context, we note that, for hexyl-chloride films,[26] dominant gauche $C_\alpha−C_\beta$ conforma-

tions could be prepared under certain conditions, which was not the case for the smaller homologs.

It would be premature to speculate about the structural implications of this relaxation behavior. At the least, it is conceivable that similar mechanisms as in the case of ethanol dimer are at play. Compact, folded structures are most likely to be among the stable isomers, and they may profit from gauche OH donor conformations. Interestingly, there is also an alternation in the Ar nanomatrix shift for the dimers. This time, the odd-membered C-chains show a larger shift than the even-membered alcohols. The nanomatrix shift is significantly larger than that of the monomer, which was not the case for ethanol dimer. For example, in propanol, it amounts to 26 cm^{-1}, twice the monomer value. The small matrix shift in ethanol dimer was interpreted as a consequence of conformational change upon Ar coating.[15] Such a change may be absent in the longer alcohols, at least for odd-membered chains. In any case, the pronounced chain size alternation is indicative of folded dimer structures.

Although Raman spectra do not contain complementary information for the dimer donor range and are hampered by a lack of substantial intensity enhancement upon hydrogen bonding, they can still provide independent evidence for the dimer complexity close to the nozzle exit. Figure 9 shows the very weak dimer scattering signals for ethanol to hexanol. Although the S/N ratio is poor, the agreement with the IR spectra even in fine detail is remarkable. A detailed comparison is found in Table 5. The same number of bands and even a similar intensity distribution is found for the He expansions. An
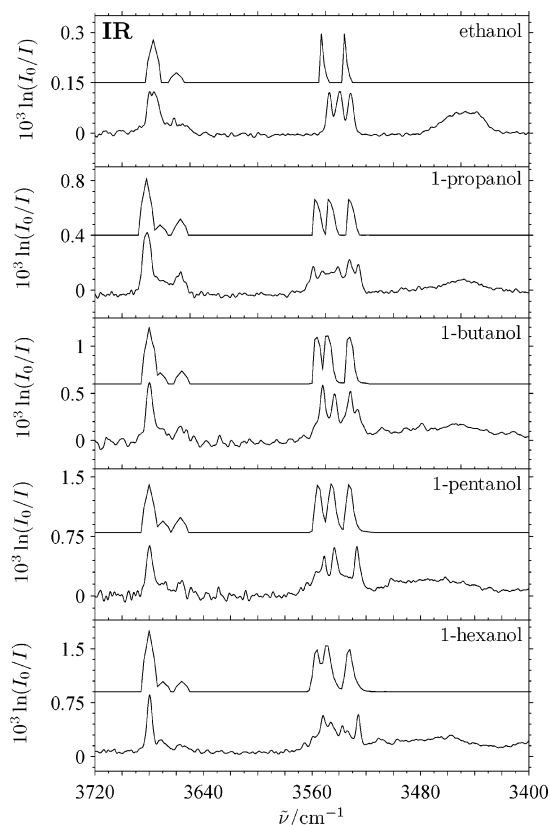
n-Alkanol Structure, Ar Coating, and Dimerization

J. Phys. Chem. A, Vol. 111, No. 31, 2007 **7447**

Figure 10. Comparison between experimental (lower trace) and theoretical IR spectra based on the AMBER model (upper trace) of the *n*-alkanols ethanol through 1-hexanol. The experimental ethanol spectrum is taken from ref 15.

advantage of Raman spectra is the better visibility of dimer acceptor bands in the neighborhood of the monomer transitions. The persistent bands near 3675 cm^{-1} and 3655 cm^{-1} are likely to have a trans and gauche dimer acceptor origin, respectively, but a more systematic investigation will have to be carried out in this context.

As a detailed theoretical modeling of dimer OH stretching spectra of alcohols is currently out of reach, we explore a zeroth order approach. Figure 10 compares simulated spectra based on the AMBER model described in section 2 with experimental IR spectra. We recall that this involves a simple mapping of the monomer profile onto the dimer region, allowing for scrambled abundances and for some spectral broadening caused by and simulated with different possible dimer conformations. Although the predicted dimer spectra are too structured, their overall widths and positions match the experimental spectra quite nicely. This indicates that the spectral spread among the dimer conformations may be largely dominated by the corresponding spread observed for the monomer frequencies. The latter increases significantly from ethanol to propanol. This is probably a consequence of C$_\gamma$ hydrogen atoms, as suggested by the 3P model in section 3. Furthermore, it confirms that the dimerization shift does not depend sensitively on the length of the chain. The simple model cannot provide a conformational assignment of the different monomer or dimer bands. Not unexpectedly, it also falls short of reproducing the detailed band structure in the dimer absorption profile.

5. Conclusions and Outlook

From the combined infrared and Raman study of linear alcohol molecules R−CH$_2$−CH$_2$−OH and their dimers and

backed by exploratory model calculations, we can draw the following robust conclusions about the structure, energetics, and dynamics of these functionalized alkyl chains:

(i) The OH stretching fundamental is sensitive to the conformation around the adjacent C−O bond and to a lesser degree also around the neighboring C−C bond. A simple model can reproduce the essential features.

(ii) The OH group favors a trans orientation with respect to the first C−C bond in the isolated molecules, although several gauche conformations are energetically competitive.

(iii) The first C−C bond favors a gauche orientation of the attached groups by a small energy margin, most likely due to a favorable oxygen lone pair interaction with C$_\gamma$−H. Such weak interactions are also crucial for chiral recognition phenomena between molecules.[51]

(iv) Despite the lack of symmetry, IR and Raman spectra of alcohol monomers and dimers provide nicely complementary information on structural isomerism. A simple model can reproduce the essential dimerization effects in the spectrum.

(v) Vibrational spectra extend the molecular size regime of accurate MW analysis to larger systems, by making use of coarse-grained spectral analogies.

(vi) An OH group attached to an even-membered alkyl chain is perturbed more strongly by a surrounding Ar nanomatrix than in the case of an odd-membered alkyl chain. For hydrogen-bonded dimers, the opposite is the case.

(vii) The conformation of alcohol molecules is more sensitive to aggregation than that of alkanes[1] or fluoroalcohols.[43] The chain length dependence of the first aggregation step is crucial for a detailed understanding of extended materials such as membranes and crystals.

In future studies, we will investigate lower frequency fundamentals which offer more sensitive and far-reaching probes of the alkyl chain conformation,[4,25,35,52] in particular in matrix isolation experiments.[16,17] Cluster size discrimination will typically be more difficult, but a combination of Raman[36] and FTIR spectroscopy[9] as well as the correlation among different frequency ranges should provide sufficient constraints for an unambiguous interpretation, at least for shorter chains. Furthermore, IR hole-burning experiments in cryogenic matrices show promise in providing a better understanding of the subtle conformational equilibria in *n*-alkanols.[16,17,20] This is a prerequisite for the study of the more complex branched[28] and fluorinated[43] alcohols.

References and Notes

(1) Kanesaka, I.; Snyder, R. G.; Strauss, H. L. *J. Chem. Phys.* **1986**, *84*, 395−397.

(2) Ly, H. V.; Longo, M. L. *Biophys. J.* **2004**, *87*, 1013−1033.

(3) Stanners, C. D.; Du, Q.; Chin, R. P.; Cremer, P.; Somorjai, G. A.; Shen, Y.-R. *Chem. Phys. Lett.* **1995**, *232*, 407−413.

(4) Tasumi, M.; Shimanouchi, T.; Watanabe, A.; Goto, R. *Spectrochim. Acta* **1964**, *20*, 629−666.

(5) Wilson, L.; Bicca de Alencastro, R.; Sandorfy, C. *Can. J. Chem.* **1985**, *63*, 40−45.

(6) Fang, Z.; Ionescu, P.; Chortkoff, B. S.; Kandel, L.; Sonner, J.; Laster, M. J.; Eger, E. I., II. *Anesth. Analg.* **1997**, *84*, 1042−1048.

(7) Sangster, J. *Octanol-Water Partition Coefficients: Fundamentals and Physical Chemistry*; Wiley Series in Solution Chemistry; John Wiley & Sons: Chichester, 1997; Vol. 2.

(8) Lutz, B. T. G.; van der Maas, J. H. *J. Mol. Struct.* **1997**, *436−437*, 213−231.

(9) Häber, T.; Schmitt, U.; Suhm, M. A. *Phys. Chem. Chem. Phys.* **1999**, *1*, 5573−5582.

(10) Provencal, R. A.; Casaes, R. N.; Roth, K.; Paul, J. B.; Chapo, C. N.; Saykally, R. J.; Tschumper, G. S.; Schaefer, H. F., III. *J. Phys. Chem. A* **2000**, *104*, 1423−1429.

(11) Rice, C. A.; Borho, N.; Suhm, M. A. *Z. Phys. Chem.* **2005**, *219*, 379−388.

(12) Borho, N.; Suhm, M. A.; Le Barbu-Debus, K.; Zehnacker, A. *Phys. Chem. Chem. Phys.* **2006**, *8*, 4449−4460.

(13) Ventola, L.; Ramirez, M.; Calvet, T.; Solans, X.; Cuevas-Diarte, M. A.; Negrier, P.; Mondieig, D.; van Miltenburg, J. C.; Oonk, H. A. J. *Chem. Mater.* **2002**, *14*, 508−517.

(14) Cézard, C.; Rice, C. A.; Suhm, M. A. *J. Phys. Chem. A* **2006**, *110*, 9839−9848.

(15) Emmeluth, C.; Dyczmons, V.; Kinzel, T.; Botschwina, P.; Suhm, M. A.; Yánez, M. *Phys. Chem. Chem. Phys.* **2005**, *7*, 991−997.

(16) Coussan, S.; Boutellier, Y.; Perchard, J. P.; Zheng, W. Q. *J. Phys. Chem. A* **1998**, *102*, 5789−5793.

(17) Coussan, S.; Alikhani, M. E.; Perchard, J. P.; Zheng, W. Q. *J. Phys. Chem. A* **2000**, *104*, 5475−5483.

(18) Choi, M. Y.; Douberly, G. E.; Falconer, T. M.; Lewis, W. K.; Lindsay, C. M.; Merritt, J. M.; Stiles, P. L.; Miller, R. E. *Int. Rev. Phys. Chem.* **2006**, *25*, 15−75.

(19) Vaden, T. D.; Lisy, J. M.; Carnegie, P. D.; Pillai, E. D.; Duncan, M. A. *Phys. Chem. Chem. Phys.* **2006**, *8*, 3078−3082.

(20) Lotta, T.; Murto, J.; Räsänen, M.; Aspiala, A. *Chem. Phys.* **1984**, *86*, 105−114.

(21) Ohno, K.; Yoshida, H.; Watanabe, H.; Fujita, T.; Matsuura, H. *J. Phys. Chem.* **1994**, *98*, 6924−6930.

(22) Ramirez-Cardona, M.; Ventola, L.; Calvet, T.; Cuevas-Diarte, M. A.; Rius, J.; Amigo, J. M.; Reventos, M. M. *Powder Diffr.* **2005**, *20*, 311−315.

(23) Jarmelo, S.; Maiti, N.; Anderson, V.; Carey, P. R.; Fausto, R. *J. Phys. Chem. A* **2005**, *109*, 2069−2077.

(24) Wandschneider, D.; Michalik, M.; Heintz, A. *J. Mol. Liq.* **2006**, *125*, 2−13.

(25) Baonza, V. G.; Taravillo, M.; Cazorla, A.; Casado, S.; Cáceres, M. *J. Chem. Phys.* **2006**, *124*, 044508.

(26) Snyder, R. G.; Schachtschneider, J. H. *J. Mol. Spectrosc.* **1969**, *30*, 290−309.

(27) Boese, R.; Weiss, H.-C.; Bläser, D. *Angew. Chem., Int. Ed.* **1999**, *38*, 988−992.

(28) King, A. K.; Howard, B. J. *J. Mol. Spectrosc.* **2001**, *205*, 38−42.

(29) Maeda, A.; De Lucia, F. C.; Herbst, E.; Pearson, J. C.; Riccobono, J.; Trosell, E.; Bohn, R. K. *Astrophys. J., Suppl. Ser.* **2006**, *162*, 428−435. See also abstract RI14, 61st Molecular Spectroscopy Symposium, Columbus, OH, June 2006.

(30) Abdurakhmanov, A. A.; Ismailzade, G. I. *J. Struct. Chem.* **1987**, *28*, 238−243.

(31) Quade, C. R. *J. Mol. Spectrosc.* **2000**, *203*, 200−202.

(32) Farrell, Jr., J. T.; Suhm, M. A.; Nesbitt, D. J. *J. Chem. Phys.* **1996**, *104*, 9313−9331.

(33) Kahn, K.; Bruice, T. C. *Chem. Phys. Chem.* **2005**, *6*, 487−495.

(34) Herman, M.; Georges, R.; Hepp, M.; Hurtmans, D. *Int. Rev. Phys. Chem.* **2000**, *19*, 277−325.

(35) Häber, T.; Schmitt, U.; Emmeluth, C.; Suhm, M. A. *Faraday Discuss.* **2001**, *118*, 331−359 and contributions to the discussion on pp 53, 119, 174−175, 179−180, 304−309, 361−363, and 367−370.

(36) Zielke, P.; Suhm, M. A. *Phys. Chem. Chem. Phys.* **2006**, *8*, 2826−2830.

(37) Frisch, M. J.; Trucks, G. W.; Schlegel, H. B.; Scuseria, G. E.; Robb, M. A.; Cheeseman, J. R.; Montgomery, J. A., Jr.; Vreven, T.; Kudin, K. N.; Burant, J. C.; Millam, J. M.; Iyengar, S. S.; Tomasi, J.; Barone, V.; Mennucci, B.; Cossi, M.; Scalmani, G.; Rega, N.; Petersson, G. A.; Nakatsuji, H.; Hada, M.; Ehara, M.; Toyota, K.; Fukuda, R.; Hasegawa, J.; Ishida, M.; Nakajima, T.; Honda, Y.; Kitao, O.; Nakai, H.; Klene, M.; Li, X.; Knox, J. E.; Hratchian, H. P.; Cross, J. B.; Bakken, V.; Adamo, C.; Jaramillo, J.; Gomperts, R.; Stratmann, R. E.; Yazyev, O.; Austin, A. J.; Cammi, R.; Pomelli, C.; Ochterski, J. W.; Ayala, P. Y.; Morokuma, K.; Voth, G. A.; Salvador, P.; Dannenberg, J. J.; Zakrzewski, V. G.; Dapprich, S.; Daniels, A. D.; Strain, M. C.; Farkas, O.; Malick, D. K.; Rabuck, A. D.; Raghavachari, K.; Foresman, J. B.; Ortiz, J. V.; Cui, Q.; Baboul, A. G.; Clifford, S.; Cioslowski, J.; Stefanov, B. B.; Liu, G.; Liashenko, A.; Piskorz, P.; Komaromi, I.; Martin, R. L.; Fox, D. J.; Keith, T.; Al-Laham, M. A.; Peng, C. Y.; Nanayakkara, A.; Challacombe, M.; Gill, P. M. W.; Johnson, B.; Chen, W.; Wong, M. W.; Gonzalez, C.; Pople, J. A. *Gaussian 03*, revision B.03, B.04, and C.02; Gaussian, Inc.: Wallingford, CT, 2004.

(38) Larsen, R. W.; Zielke, P.; Suhm, M. A. *J. Chem. Phys.* **2007**, *126*, 194307.

(39) Wang, J. M.; Cieplak, P.; Kollmann, P. A. *J. Comput. Chem.* **2000**, *21*, 1049−1074.

(40) Ponder, J. W. *TINKER: Software Tools for Molecular Design*, Version 4.2; Washington University School of Medicine: St. Louis, MO, 2004 (available from http://dasher.wustl.edu/tinker/).

(41) Case, D.; et al. *AMBER 8*, University of California: San Francisco, 2004.

(42) Takahashi, K.; Sugawara, M.; Yabushita, S. *J. Phys. Chem. A* **2003**, *107*, 11092−11101.

(43) Scharge, T.; Häber, T.; Suhm, M. A. *Phys. Chem. Chem. Phys.* **2006**, *8*, 4664−4667.

(44) Cornell, W. D.; Cieplak, P.; Bayly, C. I.; Kollman, P. A. *J. Am. Chem. Soc.* **1993**, *115*, 9620−9631.

(45) Richter, W.; Schiel, D. *Ber. Bunsen-Ges.* **1981**, *85*, 548−552.

(46) Ruoff, R. S.; Klots, T. D.; Emilsson, T.; Gutowsky, H. S. *J. Chem. Phys.* **1990**, *93*, 3142−3150.

(47) Tasiće, U.; Alexeev, Y.; Vayner, G.; Crawford, T. D.; Windus, T. L.; Hase, W. L. *Phys. Chem. Chem. Phys.* **2006**, *8*, 4678−4684.

(48) Nasirzadeh, K.; Neueder, R.; Kunz, W. *J. Chem. Eng. Data* **2006**, *51*, 7−10.

(49) Hearn, J. P. I.; Cobley, R. V.; Howard, B. J. *J. Chem. Phys.* **2005**, *123*, 134324.

(50) Tschumper, G. S.; Morokuma, K. *J. Mol. Struct. (Theochem)* **2002**, *592*, 137−147.

(51) Su, Z.; Borho, N.; Xu, Y. *J. Am. Chem. Soc.* **2006**, *128*, 17126−17131.

(52) Liu, Y.; Weimann, M.; Suhm, M. A. *Phys. Chem. Chem. Phys.* **2004**, *6*, 3315−3319.